



Theoretical model and experimental results for the nonlinear elastic behavior of human annulus fibrosus

Diane R. Wagner^{a,b}, Jeffrey C. Lotz^{a,*}

^a *Orthopaedic Bioengineering Laboratory, Department of Orthopaedic Surgery, University of California at San Francisco, (U-470) Box 0514, 533 Parnassus Avenue, San Francisco, CA 94143-0514, USA*

^b *Department of Mechanical Engineering, University of California at Berkeley, Berkeley, CA, USA*

Accepted 29 December 2003

Abstract

The physical properties of the annulus fibrosus are critical to the intervertebral disc's biomechanical function; alterations with degeneration and aging can contribute directly to joint dysfunction and pain. A constitutive model that links the mechanical structure of the annulus to its material properties is important for many bioengineering purposes. To this end, we developed a strain energy function with separate terms to represent the matrix, the fibers, and the interactions between the constituents. Additionally, we measured the tensile and compressive stress–strain response of the annulus in the circumferential direction. We simultaneously applied the strain energy function to these new data and to data from a wide range of experimental protocols reported in the literature. By choosing experimental protocols that use an unloaded reference configuration, we developed a comprehensive formulation for the multiaxial annular elastic behavior. As a partial validation, this formulation predicted experimental results that were not included in model parameter specification. We anticipate that this constitutive formulation will be useful for computational simulations of the disc's biomechanical response and for elucidating structure–function relationships of the annulus fibrosus.

© 2004 Orthopaedic Research Society. Published by Elsevier Ltd. All rights reserved.

Keywords: Intervertebral disc; Annulus fibrosus; Strain energy; Mechanical properties; Elastic

Introduction

The annulus fibrosus is a pliant, fibrous composite tissue that forms the periphery of the intervertebral disc. Biomechanically, it serves dual roles: as a ligament to guide intervertebral motion and as a vessel wall to contain nuclear pressure. This complex function is facilitated by a composite architecture that consists of collagenous lamellae [4,14,19] with the collagen oriented at $\pm 60^\circ$ to the vertical axis at the periphery of the disc and closer to $\pm 45^\circ$ in layers adjacent to the nucleus. Within and between the lamellae is a proteoglycan-rich ground substance. This structural organization is similar to an angle-ply composite and leads to extremely anisotropic material properties.

A mathematical description of annular material behavior is important for many bioengineering purposes, yet is particularly difficult to achieve due to tissue non-

linearity and anisotropy. To facilitate model development, the tissue is generally either represented as a composite with discrete collagen fibers embedded in an isotropic matrix or as an orthotropic continuum. We have chosen to utilize a continuum approach because material properties are determined directly from experimental tissue behavior, yielding a more tractable formulation of a constitutive model. A composite continuum theory that was first proposed by Spencer [23] has been previously applied to the annulus by several researchers [7–9,17,29]. It allows for a constitutive model with a mathematical structure that reflects the composite tissue architecture. Nonlinear strain energy functions for composite tissues such as tendon [28] and artery [13] as well as for the annulus [7] have explicitly modeled the matrix and the fibers of the tissue with separate, additive terms. However, these studies did not model the mechanical contributions of interactions between the constituents, such as fiber–fiber or fiber–matrix interactions.

In order to develop a nonlinear, anisotropic constitutive model that accurately represents the stress and

* Corresponding author. Tel.: +1-415-476-7881; fax: +1-415-476-1128.

E-mail address: jlotz@itsa.ucsf.edu (J.C. Lotz).

strain states of in vivo tissue deformations, multiple experimental in vitro results must be considered. However, relying on historical experimental datasets is problematic since these have been collected at different times and by different authors and therefore may not assume the same tissue reference configuration (deformation in unstressed state). Such discrepancies can create elastic modulus discontinuities at transitions between datasets, such as the point of zero strain between tension and compression. Fitting the coefficients of a smooth curve to stress–strain data that contains a large discontinuity in the modulus may result in physically implausible theoretical predictions that are not strictly increasing [26].

Our first objective was to generate tensile and compressive experimental data with a common reference configuration when studying the circumferential stress–strain behavior of the annulus. We chose the unloaded state (no tare load) of the tissue specimens as a convenient reference configuration for these experiments and subjected the rectangular annulus fibrosus specimens to a continuous deformation that included both uniaxial tension and compression. Our second objective was to develop a constitutive formulation for the multiaxial annular elastic behavior. We accomplished this by applying a strain energy function to experimental data from this study as well as to data from the literature. We chose a strain energy function composed of individual terms to represent specific tissue features such as the matrix, the fibers, and interactions between the constituents.

Materials and methods

Tension/compression testing

Human lumbar spines were harvested at autopsy from six individuals aged 16–38 years and stored frozen (-20°C) until dissection. Two microtome blades held parallel at a set distance apart were used to produce rectangular specimens 5 mm wide, 7 mm high, and approximately 30 mm long from the anterior portion of the L4/5, L3/4, and L2/3 discs (Fig. 1) with a visually uniform cross sectional area. Only grades I and II (nondegenerate) discs [24] were used ($n = 11$). To minimize tissue swelling during testing, specimens were soaked overnight in a 0.15 M saline and protease inhibitor solution. On the day of

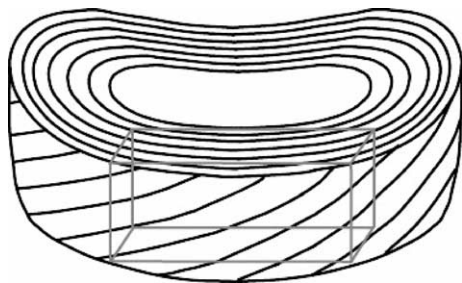


Fig. 1. Specimens were harvested from the anterior region of nondegenerate intact intervertebral discs, with the longest dimension coinciding with the circumferential direction.

testing, four stainless steel wire rods (0.635 mm \varnothing) that were to be gripped by the testing apparatus were inserted into the tissue near each end of the specimen using a custom alignment jig. Using another custom alignment jig, nine small stainless steel insect pins (0.25 mm \varnothing) were pushed through the thickness in the middle of the specimen in a grid pattern (grid dimension 3.0 \times 3.0 mm) [1,2]. Visual targets for the strain measurements were created by cutting the heads of the pins close to the tissue and painting the blunt ends black. The sharp ends of the pins were also cut close to the tissue to eliminate interference with one another or with the testing apparatus.

Any tissue specimen tested in compression should have an aspect ratio that precludes buckling. Our specimens were inhomogeneous because they were large compared to the tissue architecture. We accounted for this inhomogeneity in three ways. First, the pins went all the way through the tissue, resulting in deformations that were averaged throughout the thickness for each strain marker. Second, the tissue was tested with two different pin configurations (Fig. 2). The order of the testing was randomly predetermined, and the results of both tests were included when determining the overall characteristics of the annulus. Finally, we used nine pins in a grid pattern as strain markers and found an average tissue strain using the method described by Bass [1,2]. A pilot experiment tested the influence of repeated pin insertions on the tissue's mechanical properties. We questioned whether repeated pin insertions would damage and weaken the tissue, however the tissue was just as likely to appear stiffer after a subsequent insertion as it was to appear less stiff. We concluded that the influence of repeated insertions is insignificant when compared to other randomizing effects.

The specimens were submerged in 0.15 M saline and protease inhibitor solution during testing. The custom testing apparatus consisted of: grips to hold the wire rods; a precision force transducer (25 N Load Cell Model LCCA, Omega Engineering, Stamford, CT) to record the forces developed in the tissue; and a computer-controlled imaging system to calculate the strains in real time. Custom programs were developed (Labview and IMAQ Vision, National Instruments, Austin, TX) that: captured images of the specimen and strain measurement pins; thresholded the image to locate the pins; calculated the average strain in both the direction of applied force and transverse to the applied force; and calculated the stress (as load divided by the specimen's cross sectional area before it was submerged in saline). After the load cell was zeroed without the specimen in place, the tissue was loaded into the grips of the testing apparatus (Fig. 3) and preconditioned with 10 cycles of tension and compression (0.05 to -0.01 MPa) at a strain rate of approximately 0.002 s^{-1} . The specimen was unloaded to zero applied force; this was our reference configuration for both the tensile and compressive tests. The specimens were then tested in tension to 0.4 MPa at a strain rate of 0.0001 s^{-1} with forces and strains recorded every 2 s. After the tissue was unloaded, it was preconditioned again for five cycles of the above regime, returned to a zero-stress state, and then tested in compression to -0.04 MPa at the same strain rate. The preconditioning regime and test stress limits were

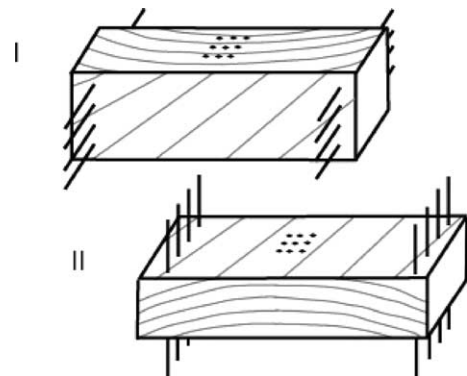


Fig. 2. Tissue was tested in two configurations to account for material inhomogeneity. The pins were inserted parallel to the lamellae in pin configuration I and through the thickness of the lamellae in pin configuration II.



Fig. 3. Stress and strains were measured with custom test apparatus. Pin configuration II is shown.

found to be repeatable and nondamaging in a pilot study. The specimen was then removed from the testing apparatus, the strain measurement pins were extracted, the tissue was rotated 90° about the long axis, and new strain measurement pins were inserted into the tissue. The specimen was returned to the testing apparatus and the above tensile and compressive protocols were repeated.

An exponential curve of the form $\sigma = \frac{A}{B}(e^{B\sigma} - 1)$ [12,16] was fit to the tensile stress–strain data from each side of each specimen with a Levenberg–Marquardt algorithm (Matlab 5.3, The Mathworks, Inc., Natick, MA), where A is the slope at the origin (in MPa), and B is a dimensionless measure of nonlinearity. Because each specimen was tested twice, two data sets for each specimen were measured and both used to calculate average coefficients (A and B). Similarly, the tangent modulus at a stress of 0.4 MPa was calculated by evaluating the derivative of the exponential equation for each side of each specimen and an overall average value was found. From the compressive experiments, a straight line (that did not necessarily pass through zero) was fit to both compression sets and used to find an overall compressive modulus and y -intercept. In addition to computing the overall averages for the above parameters, we also averaged these values separately for the two different pin configurations so that we could determine whether the inhomogeneity of the tissue affected the results. The Poisson's ratios were calculated separately for tension and compression and for each pin configuration, and were determined by plotting the strain in the direction of applied force on the x axis and the strain transverse to the applied force on the y axis and fitting a straight line to the data that passed through zero; the Poisson's ratio was the negative of the calculated slope. Because of an error in calculating the transverse strains for the first specimens, $n = 5$ for the Poisson's ratio data.

Continuum mechanics background

The constitutive equation for a Green elastic material can be written as

$$\mathbf{T} = \frac{2}{J} \mathbf{F} \frac{\partial W}{\partial \mathbf{C}} \mathbf{F}^T \quad (1)$$

where \mathbf{T} is the Cauchy stress tensor, J is the determinant of the deformation gradient tensor \mathbf{F} , the right Cauchy–Green tensor $\mathbf{C} = \mathbf{F}^T \mathbf{F}$, and $W = W(\mathbf{C})$ is the strain energy. Alternatively, we can write an expression for the first Piola–Kirchhoff stress tensor \mathbf{P} as $\mathbf{J}\mathbf{T} = \mathbf{P}\mathbf{F}^T$. The Lagrangian strain \mathbf{E} is defined as $\mathbf{E} = \frac{1}{2}(\mathbf{C} - \mathbf{I})$ where \mathbf{I} is the second order identity tensor.

We modeled the anisotropic annulus as a fiber composite continuum in which an isotropic matrix is reinforced by two systematically arranged families of fibers [23]. The fiber directions are represented by material line elements in the reference configuration, denoted by unit vectors \mathbf{a}_0 and \mathbf{b}_0 . These elements are deformed in the present configuration, and their deformed directions are represented by the unit vectors \mathbf{a} and \mathbf{b} . To model the annulus, we chose a Cartesian basis ($\mathbf{E}_1, \mathbf{E}_2, \mathbf{E}_3$) to be aligned with the radial, circumferential, and axial

directions, respectively, of a local anatomic configuration [17]. We defined

$$\mathbf{a}_0 = \sin \phi \mathbf{E}_2 + \cos \phi \mathbf{E}_3, \quad \mathbf{b}_0 = -\sin \phi \mathbf{E}_2 + \cos \phi \mathbf{E}_3 \quad (2)$$

so that the two fiber families were oriented at angles of plus and minus ϕ degrees from the axial direction in the reference configuration. We assumed that the two fiber families are mechanically equivalent such that the strain energy W is symmetric with respect to interchanging the fiber directions \mathbf{a}_0 and \mathbf{b}_0 . With these assumptions, Spencer showed that W can be expressed as a function of eight invariants:

$$W = W(I_1, I_2, I_3, I_8, I_9, I_{10}, I_{11}, \cos^2 2\phi) \quad (3)$$

where

$$\begin{aligned} I_1 &= \text{tr } \mathbf{C}, & I_2 &= 0.5[(\text{tr } \mathbf{C})^2 - \text{tr } \mathbf{C}^2], & I_3 &= \det \mathbf{C}, & I_4 &= \mathbf{a}_0 \cdot \mathbf{C} \mathbf{a}_0, \\ I_5 &= \mathbf{a}_0 \cdot \mathbf{C}^2 \mathbf{a}_0, & I_6 &= \mathbf{b}_0 \cdot \mathbf{C} \mathbf{b}_0, & I_7 &= \mathbf{b}_0 \cdot \mathbf{C}^2 \mathbf{b}_0, & I_8 &= \cos 2\phi \mathbf{a}_0 \cdot \mathbf{C} \mathbf{b}_0, \\ I_9 &= I_4 + I_6, & I_{10} &= I_4 I_6, & I_{11} &= I_5 + I_7 \end{aligned} \quad (4)$$

and 2ϕ is the angle between the fiber families in the reference configuration.

Strain energy specification

We chose a strain energy function for a fiber composite that derives its mechanical response from three distinct components: an isotropic matrix, two highly oriented fiber populations, and interactions between the other components, such as between the fibers or between the matrix and the fibers:

$$W = W_{\text{matrix}} + W_{\text{fibers}} + W_{\text{interactions}} \quad (5)$$

We associated the matrix contribution W_{matrix} with an isotropic mechanical response. Noting that I_1, I_2 , and I_3 are the invariants for an isotropic material, we assumed that the strain energy contribution of the matrix would be a function of these invariants. We modeled the response of the matrix with two separate additive terms: a spherical (volumetric) term which is a function only of I_3 , and a deviatoric (distortional) term which is a function of $I_1 I_3^{-1/3}$, the deviatoric form of the first invariant of \mathbf{C} . The invariant I_2 was not used. Thus, we wrote

$$W_{\text{matrix}} = W_{\text{matrix-spherical}}(I_3) + W_{\text{matrix-deviatoric}}(I_1 I_3^{-1/3}) \quad (6)$$

To model the fiber term W_{fiber} of the strain energy, we utilized a measure of the fiber stretch in the \mathbf{a} and \mathbf{b} directions. The invariant I_9 can be written as $I_9 = \lambda_a^2 + \lambda_b^2$ (λ_a is the stretch in the \mathbf{a} direction; λ_b is the stretch in the \mathbf{b} direction) and is the invariant that most directly measures the stretch of the fibers. For this reason, we wrote the fiber term in Eq. (5) as a function of I_9 :

$$W_{\text{fiber}} = W_{\text{fiber}}(I_9) \quad (7)$$

The interactions term represents fiber–fiber and fiber–matrix interactions. However, we assumed that the effect of collagen crosslinks would dominate this term because the contribution of the collagen–matrix interactions would be weak in comparison. We therefore designed the interactions term to specifically model collagen crosslinks. We further assumed that the crosslinking occurs between collagen fibers within a lamella and serves to constrain the fibers from sliding past one another. Given these assumptions, the mechanical response of collagen crosslinks is a resistance to shear in the direction of the fibers in the lamellar plane. Correspondingly, we wrote the interactions term of the strain energy as a function of the shear strain in the two fiber directions. In the plane of the fibers, the shear strain along the fiber directions \mathbf{a} and \mathbf{b} can be written as a function of the principle Lagrangian strains through a Mohr's circle analysis. Since the experimental protocols are pure stretch deformations, the three principal Lagrangian strains are the diagonal components of the strain matrix \mathbf{E} , and the shear strains in the two directions are equal. We wrote

$$\gamma_a = \gamma_b = \frac{1}{2}(E_{22} - E_{33}) \sin 2\phi \quad (8)$$

where γ_a and γ_b are the shear strains in the direction of \mathbf{a} and \mathbf{b} in the plane of the fibers. Because we expect the strain energy to be positive for both positive and negative shear strains, the interactions term must be an even function of γ_a and γ_b , for example γ_a^2 and γ_b^2 . Using the

definition of \mathbf{E} and the form of the invariants in Eq. (4), we determined that γ_a^2 can be written as a function of Spencer's invariants:

$$\gamma_a^2 = I_5 - I_4^2 \quad (9a)$$

and for a two fiber family

$$\gamma_a^2 + \gamma_b^2 = I_{11} - I_9^2 + 2I_{10} = I_{11} - I_4^2 - I_6^2 \quad (9b)$$

The interactions term was written as a function of the shear strains in the two fiber directions:

$$W_{\text{interactions}} = W_{\text{interactions}}(I_{11} - I_9^2 + 2I_{10}) \quad (10)$$

The strain energy function given by (3) was therefore reduced to one that is the sum of four terms with each term representing one of the three material components and each term dependent only on one variable.

The particular form of each term was chosen to match the experimentally observed mechanical behavior of the corresponding annular constituent. Additionally, each term was written so that the stress contribution in the undeformed state would be zero, automatically giving a stress-free reference configuration. We chose to model the spherical term of the proteoglycan matrix with

$$W_{\text{matrix-spherical}}(I_3) = a_1(I_3 - 1/I_3)^2 \quad (11)$$

so that the strain energy approaches infinity as the determinate of \mathbf{F} approaches both zero and infinity. The deviatoric portion of the matrix strain energy was modeled with the term

$$W_{\text{matrix-deviatoric}}(I_1 I_3^{-1/3}) = a_2(I_1 I_3^{-1/3} - 3)^2 \quad (12)$$

To capture the strongly nonlinear response of the collagen fibers and to provide a mechanical response that is much stiffer in tension than in compression, we used a modified exponential term for the strain energy response of the collagen fibers:

$$W_{\text{collagen}}(I_9) = \frac{a_3}{b_3} (e^{b_3(I_9 - 2)} - b_3 I_9) \quad (13)$$

For the interactions term, we again chose an exponential form:

$$W_{\text{interactions}}(I_{11} - I_9^2 + 2I_{10}) = \frac{a_4}{b_4} e^{b_4(I_{11} - I_9^2 + 2I_{10})} \quad (14)$$

The coefficients a_1 , a_2 , a_3 , and a_4 all have units of MPa, while the coefficients b_3 and b_4 are dimensionless.

Using Eq. (1) and the particular form of the strain energy function proposed in (11)–(14), we used Mathematica (Wolfram Research, Champaign, IL) to write an explicit expression for the Cauchy stress in terms of the principal stretches, the six coefficients of the strain energy function, and the fiber directions. The resulting stress–stretch constitutive equation is too long to present here.

Experimental data

To determine values of the coefficients found in the strain energy function that are specific to the annulus, we applied the strain energy function to data from a number experimental protocols that span a wide range of annular deformations. We chose experimental protocols that applied little or no tare load in order to avoid large discrepancies in tangent modulus at the tension/compression transition. The experimental data consisted of: (A) uniaxial tension in the radial direction, nondegenerate anterior middle [10]; (B) uniaxial tension in the circumferential direction, nondegenerate anterior middle (present study); (C) uniaxial tension in the axial direction, nondegenerate anterior-lateral outer [5]; (D) unconfined compression in the circumferential direction, nondegenerate anterior middle (present study); (E) confined compression in the radial direction, nondegenerate lateral middle [18]; (F) confined compression in the axial direction, nondegenerate lateral middle [18]; and (G) biaxial tension, axial stress versus axial stretch with circumferential stretch held constant at $\lambda_2 = 1.0$, nondegenerate anterior outer [1,2]. We assumed that these experimental data represent the equilibrium elastic response of the tissue and that the deformations were homogeneous.

The stress in any one direction depends on all three principal stretches. Therefore, for the experimental protocols (A)–(G) we had to describe the three principal stretches although all were not directly measured. In using the data from (A), we wrote that $\lambda_2 = 1.35 - 0.35\lambda_1$ where stretch in the radial direction, λ_1 , was measured. We chose

Poisson's ratio $\nu_{12} = 0.35$ because it is within one standard deviation of experimental measurements [9] and led to thermodynamically permissible results. Because the collagen fibers support a compressive load for experiment (A) and are weak in compression, we assumed that the stretch response of the axial direction is similar to that of the circumferential direction and estimated that $\lambda_3 = 1.35 - 0.35\lambda_1$ as well. In experiments (B) and (C), a preliminary analysis indicated that the overall statistical fit was extremely sensitive to the amount of lateral contractions in the plane of the fibers; consequently we considered ν_{23} and ν_{32} to be material parameters best determined through the statistical nonlinear fitting algorithm. Experimental mean values of $\nu_{21} = 0.33$ and $\nu_{31} = 0.14$ have been reported [9], in other words $\lambda_1 = 1.33 - 0.33\lambda_2$ for (B) and $\lambda_1 = 1.14 - 0.14\lambda_3$ for (C). For the unconfined compression experiment (D), we used results from the current study, $\nu_{21} = 0.73$ and $\nu_{23} = 0.87$. In the confined compression experiments (E) and (F), we set the stretches in the two directions that were normal to the loading direction equal to unity; i.e. $\lambda_2 = \lambda_3 = 1.0$ for (E) and $\lambda_1 = \lambda_2 = 1.0$ for (F). When writing the biaxial equations for experiment (G), we assumed that the contraction in the radial direction would be greater than for the uniaxial experiments (B) and (C). We therefore estimated that $\lambda_1 = 1.5 - 0.5\lambda_3$. We also set $\lambda_2 = 1.0$, matching experimental boundary conditions. For the five experiments (A)–(D) and (G) we converted the equation for Cauchy stress to the first Piola–Kirchhoff stress \mathbf{P} , since experimental stresses were calculated by normalizing the measured force by the original cross sectional areas. A preliminary analysis showed that the overall statistical fit was extremely sensitive to the fiber angle, ϕ , therefore we assumed a uniform fiber angle from the axial direction but considered ϕ to be a parameter best found through the statistical fitting algorithm.

In addition to conducting the simultaneous regressions to all the experimental data sets in the direction of applied stress, we also invoked the traction-free boundary conditions for (A)–(D). In general, when solving the boundary value problem for the radial tension test (A) the free surface stresses in the circumferential and axial directions T_{22} and T_{33} must equal zero. When considering the traction-free boundary conditions for (A), we derived equations for the circumferential and axial stresses, T_{22} and T_{33} , in terms of the radial stretch, λ_1 and included them in the set of equations used in the simultaneous regression. Similarly, we included equations for the traction-free faces in circumferential tension (B) and compression (D) as functions of λ_2 and in axial tension (C) as functions of λ_3 .

For each experiment (A)–(G) we substituted our assumptions about the stretches in the lateral directions into the expressions for stress to obtain equations for the principal stresses as a function of the stretch in the direction of applied stress. We used 15 equations in the nonlinear regression: from (A)–(D) we used one stress–stretch equation for the direction of loading and two zero-stress equations each; from confined compression experiments (E) and (F) we used the stress–stretch equation in the direction of applied loading; and from biaxial tension (G) we used only the stress–stretch equation in the axial direction (the direction of increasing stretch). The dataset to which we conducted the simultaneous regression consisted of stretch–stress data and entries for the zero stress equations. Because the fitting algorithm for the nonlinear regression seeks to minimize the overall absolute error in the predicted stresses, the experimental data with higher stresses would have been effectively weighted more heavily if the data had not been scaled. To account for this, the stress–stretch data for each experiment was scaled by its experimental standard deviation. This technique more heavily weighted experimental data that were consistent across multiple specimens [20].

Material parameter determination and validation

To prescribe the material parameters a_1 , a_2 , a_3 , b_3 , a_4 , b_4 , ν_{23} , ν_{32} , and ϕ imbedded in our formulation, we conducted a simultaneous nonlinear regression to the mean response of the stress versus stretch datasets as well as traction-free datasets using a modified Levenberg–Marquardt nonlinear fitting algorithm (PV-Wave, Visual Numerics, San Ramon, CA). This was accomplished through the technique of Klich and Lotz [17], which used a composite function T^* that was a sum of all 15 equations from the seven experimental protocols:

$$T^* = \sum_{i=1}^{15} m_i T_i \quad (15)$$

where T_i is the i th equation that we considered, and m_i is an “accounting variable” which is either 1 or 0. Material coefficients were determined by fitting this composite function to a composite dataset that included stress–stretch or zero-stress data for each of the 15 equations. In addition to stretch and stress data, our dataset also includes values for each m_i . Each datum point that we consider is associated with only one of the 15 equations; the corresponding m_i is 1, and all other m_i are 0. In this way we individually and simultaneously determined the best fit of our material parameters to all the experimental data.

To validate in part the model and the values of the coefficients that were determined, we predicted stress–stretch results that had not been included in the above simultaneous statistical fit. Although the axial stress in biaxial tension was included in the overall regression, the circumferential stress in biaxial tension was not, and was used to validate the model instead. We wrote an expression for the circumferential stress in the biaxial test protocol with the circumferential stretch held at 1.0. Similar to experiments that were included in the nonlinear regression, we had to make assumptions about the stretch of the tissue in every direction during the biaxial protocol in order to predict the circumferential stress. As with experiment (G), we estimated that $\lambda_1 = 1.5 - 0.5\lambda_3$ and set $\lambda_2 = 1.0$. Using the best-fit values of the material parameters from the previous simultaneous fit, we determined the theoretical stress–stretch prediction for the circumferential stress in biaxial tension and compared our theoretical prediction to the experimental data.

Results

We found that the annulus has a significant toe region in tension, which facilitates the smooth transition between the soft compressive behavior and the stiff tensile behavior at higher strains. The exponential equation represented the nonlinear tensile circumferential behavior well, with a correlation coefficient >0.95 for all tests (Fig. 4). The average tensile behavior was characterized by $A = 0.447 \pm 0.379$ MPa and $B = 31.9 \pm 12.2$. The average slope at a stress of 0.4 MPa was 13.2 ± 5.00 MPa. A straight line was a sufficient representation of the compressive stress–strain behavior, with $R^2 > 0.90$ for all tests. The average slope for the compressive experiments

was 0.235 ± 0.127 MPa. The average y intercept was small at -0.00349 ± 0.00533 MPa. This nonzero result is due to the fact that the tissue did not return exactly to the reference configuration (zero-stress state after the last preconditioning cycle) at the start of the compressive testing. We found no significant difference between the two pin configurations in the mean values of any of the five parameters that we studied ($p > 0.1$ for all, data not shown), which implies that our methods to measure strain sufficiently eliminated inhomogeneity effects.

The measured Poisson’s ratios were: $\nu_{21} = 0.40 \pm 0.15$ in tension and 0.73 ± 0.21 in compression, and $\nu_{23} = 2.32 \pm 0.87$ in tension and 0.87 ± 0.49 in compression. The mean Poisson’s ratios for the tensile tests were within one standard deviation of previously reported data [9], but because of our small sample size, we used the previously reported value of ν_{21} in developing the equations for the circumferential uniaxial tension test (B), while ν_{23} was found through the statistical fit. For both Poisson’s ratios, the value that we measured in tension was significantly different from the value we measured in compression ($p < 0.05$ for ν_{21} and $p < 0.025$ for ν_{23}), therefore we used our measured compressive Poisson’s ratios in the unconfined compression experiment (D) as we felt that they were more accurate than previously reported Poisson’s ratios that had been based on tensile experiments. The difference in tensile and compressive Poisson’s ratios has not been previously reported, but is expected because components of the annulus, such as collagen fibers, behave differently in tension and compression.

The best fit values for the nine material parameters of the strain energy function $\{a_1, a_2, a_3, b_3, a_4, b_4, \nu_{23}, \nu_{32}, \phi\}$ were $\{0.0772, 0.00432, 0.00699, 26.3, 0.00812, 11.2, 1.63, 0.412, 55.6^\circ\}$ and could be determined from a wide range

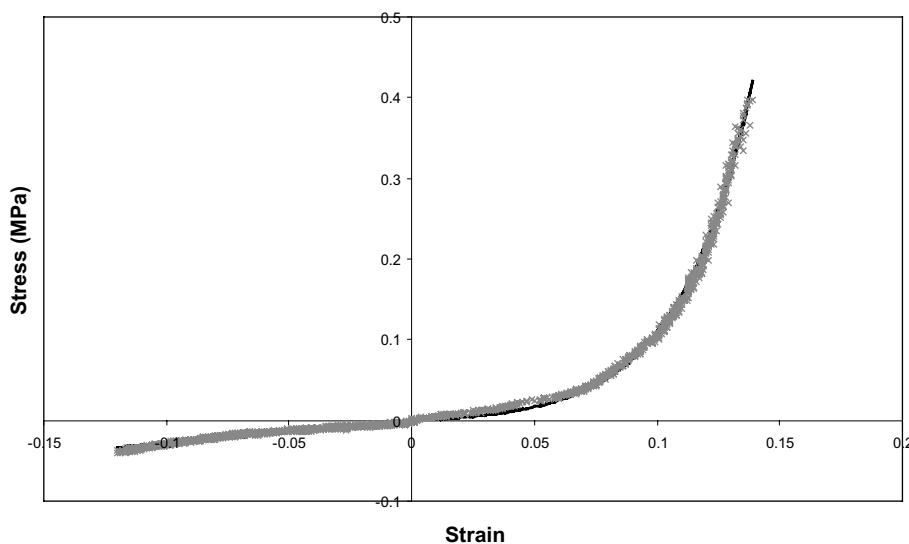


Fig. 4. Representative experimental data show that the nonlinear tensile circumferential behavior was well represented by an exponential equation $\sigma = \frac{A}{B}(e^{B\epsilon} - 1)$ and that a straight line sufficiently represented the compressive stress–strain behavior.

of starting values, suggesting that these values may be unique. These coefficients resulted in stress–stretch curves that lay within one standard deviation for all experimental deformations (Fig. 5). The equations for the traction-free faces had been fit to zero stress in the simultaneous regression, therefore a good fit for these equations is one in which the predicted stress is nearly zero. In circumferential and axial tension experiments (B) and (C), the predicted stresses on the traction-free faces are very small, particularly when compared to the

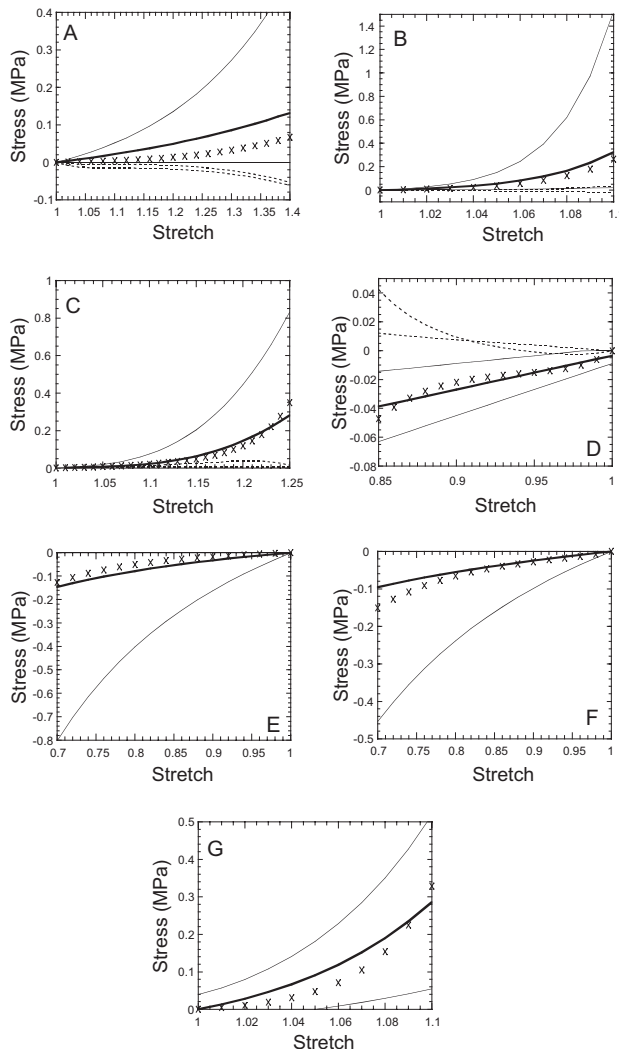


Fig. 5. Results of the simultaneous curve-fit to the measured stress–stretch data and the eight additional equations representing the two traction-free boundary conditions for each experiment A–D. A = radial tension [10]; B = circumferential tension (current study); C = axial tension [5]; D = unconfined circumferential compression (current study); E = radial confined compression [18]; F = axial confined compression [18]; G = biaxial tension in the axial direction, circumferential stretch = 1.0 [1,2]. Solid curves = mean experimental response \pm 1 std dev; \times = theoretical fit to measured stress–stretch response; dashed lines = theoretical description of traction-free stress–stretch response for experiments A–D.

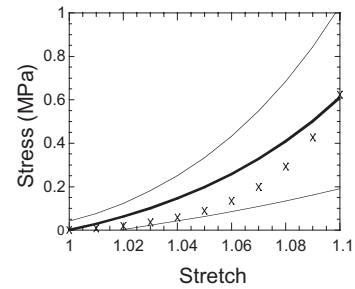


Fig. 6. The model and best fit coefficients predicted to within one std dev the biaxial behavior in the axial direction. Black lines: mean experimental behavior \pm 1 std dev [1,2]; \times 's: theoretical prediction.

applied stress. The predicted stresses on the traction-free faces in the radial tension test (A) and the circumferential compression test (D) are of a similar magnitude but appear large compared to the compliant response in the direction of applied stress.

Although ν_{23} , ν_{32} , and ϕ have been measured experimentally, the variation in the measured data is large, and our results were sensitive to these parameters, motivating us to determine these values through the statistical fitting algorithm. Our model prediction $\nu_{23} = 1.63$ was within one standard deviation of experimental values but our prediction of $\nu_{32} = 0.412$ was slightly below that observed experimentally [9]. The prediction $\phi = 55.6^\circ$ is reasonable given that the experimental data were taken from both the outer and middle annulus. We used the above material parameters to predict the stress–stretch response of experimental data that had not been included in the statistical fit. Specifically, we predicted the response to biaxial tension in the circumferential direction (circumferential stretch $\lambda_2 = 1.0$) to within one standard deviation of the experimental data (Fig. 6).

Discussion

Our experimental results demonstrate that the annulus fibrosus material response is essentially continuous through 0% strain and that the annulus has a significant toe region in tension in the circumferential direction. These results are consistent with those found in the axial direction [5] and contribute to a set of experimental data that can be used to determine an orthotropic, nonlinear constitutive law. To this end, we developed a strain energy function with separate terms to represent the contributions from annular constituents that accurately matches the mean response to multiple experimental deformations. In addition, we used this constitutive formulation to predict the response to biaxial tension in the circumferential direction to within one standard deviation.

The experimental data highlight the significance of reference configuration selection to the material response of soft tissues, which typically exhibit a toe region in tension. The toe region of the annulus may be a feature of the material behavior that is of particular interest because of its similarity to the neutral zone that is seen for many loading conditions of the intervertebral disc [21]. Depending on the research question being addressed, misrepresentation of the toe region can have deleterious consequences when quantifying the annular material response. We calculated the impact of a 0.005, 0.01, and 0.02 MPa tare load on the average tensile stress–strain behavior of the annulus. As expected, the toe region decreased for an increasing tare load, and the stress–strain curve shifted to the left (Fig. 7). The exponential $\sigma = \frac{A}{B}(e^{Be} - 1)$ still represented the data well, but the values of the coefficients, and in particular A (the initial modulus), changed dramatically, introducing significant error. For example, a tare load of 0.02 MPa resulted in a 148% error in the determination of A , and more seriously, in a 26% error in the strain at a stress of 0.4 MPa. On the other hand, the same tare load resulted in only an 8% error in the tangent modulus at 0.4 MPa.

The analysis of the effect of an initial tare load on the material behavior is helpful when we compare the current study to a previously reported tensile protocol that applied a small tare load at the start of the test [6]. In addition to the tare load that was applied in this previous protocol, the reference configuration in this previous study differed from ours by our choice of preconditioning regime (which included both tension and compression) and by our decision to soak the tissue overnight in saline. Although soaking was necessary to equilibrate swelling effects, it likely had a significant impact on our measured material properties. However, we hypothesized that swelling would decrease the length of the toe region because the collagen fibers would be in

a state of increased tension. Instead, our data showed a more significant toe region, a much lower initial tensile modulus, and a higher strain for a given stress compared to the previously reported data [27]. However, we observed no significant difference in tangent modulus ($p > 0.1$) away from the toe region, demonstrating that we are observing the same mechanical behavior at higher tensile strains and that the results of the two studies are consistent. These data are a reminder, however, that a single parameter, such as a tangent modulus, cannot fully characterize the behavior of nonlinear materials.

Previous uniaxial experiments in the circumferential direction demonstrated a discontinuity in the elastic modulus at 0% strain [6,18], most likely because the data originated from two different experimental protocols (tension and compression) that did not use the same reference configuration. Although the results of the current study visually appear to predict a continuous elastic modulus, our data showed a small but significant difference in tensile and compressive moduli (0.447 ± 0.379 MPa versus 0.235 ± 0.127 MPa) at 0% strain ($p < 0.025$). This discontinuity is likely an artifact of our experimental protocol, as we measured the tensile and compressive responses sequentially rather than continuously. Also, we described the tensile behavior with an exponential equation that fit the data well but may not optimally fit the behavior near 0% strain. Similarly, the compressive behavior was described well by a straight line, but the behavior near 0% strain may not have been accurately captured in the overall linear regression. Regardless, the experimental results from the current study are an improvement for those attempting to write an annular strain energy function for both tension and compression. By using experimental protocols which all minimized the tare load, we eliminated our previous mathematical difficulties and determined theoretical fits for seven distinct deformations that include both tension and compression to within one standard deviation of the experimental means. The small discontinuity in the circumferential modulus did not lead to physically implausible theoretical fits.

We used a continuum composite theory to develop a strain energy function with separate terms to represent the contributions of the matrix, the fibers, and the interactions between these components. Although Quapp and Weiss [22] postulated that the existence of a fiber–matrix term is “presumed to take the form of a shear coupling between the matrix and the fibers”, to our knowledge the current study is the first to develop a specific mathematical form for the mechanical contributions of an interaction constituent. We used our proposed form of an annular strain energy function to predict the experimental circumferential stress in biaxial tension with the circumferential stretch held equal to one. This represents an extrapolation of the model to results other than those

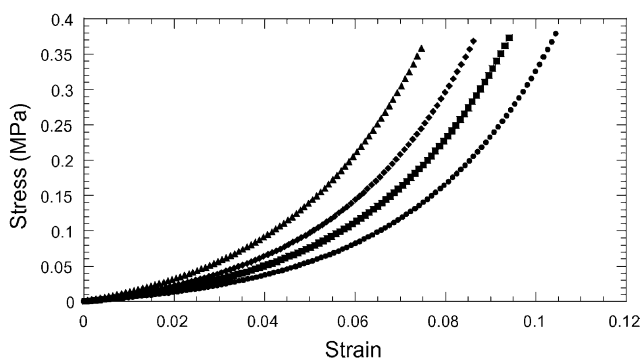


Fig. 7. The impact of a 0.005, 0.01, and 0.02 MPa tare load on the average tensile stress–strain behavior in the circumferential direction. (●) no pre-load, (■) 0.005 MPa pre-load, (◆) 0.01 MPa pre-load, and (▲) 0.02 MPa pre-load.

included in the nonlinear regression. Previous annular models [17] have been unsuccessful in predicting experimental behavior that had not been included in the simultaneous fit. A mechanistic strain energy function which models the mechanical response of the tissue's structural components may better predict the complex in vivo physiologic behavior than a purely phenomenological model. Of course, the current model has not been fully validated. In particular, improved model predictions of the experimentally measured Poisson's ratio ν_{32} [9] and comparisons with shear experimental data [11,15] have been left for a future study.

The tractable formulation of the interactions term was predicated on some simplifying assumptions. First, we assumed that the mechanical response of the annulus derives from only three constituents: an isotropic matrix, fibers that are oriented in a particular direction, and interactions that are restricted to fiber crosslinking. In reality, the architecture of the annulus is complex, and many effects are not represented in the model. Additionally, each category represents the mechanical contribution from many macromolecules or their interactions, not just one. For example, the interactions term likely represents some fiber–matrix interactions as well as collagen crosslinks. However, since the modulus of the matrix is small compared to the modulus of the collagen fibers, we expect that the collagen–matrix interactions will also be small in comparison to the collagen crosslinks and that the effect of the crosslinks will dominate this term. The impact of this assumption is unclear, as the mechanical role of fiber–matrix interactions in collagenous tissues has been reported only for an articular cartilage study. This study demonstrated that the fiber–matrix interactions have only a minor effect on the transverse cohesive strength of cartilage, suggesting that fiber–fiber linkages play a more consequential role [3]. A second fundamental assumption we made was that collagen crosslinks occur primarily between fibers that are within a lamella rather than between fibers of adjacent lamellae. This assumption allowed us to confine the effect of the crosslinks to the plane of the fibers. Although the collagen fibers are primarily associated with a particular lamella, fiber interlacing between the lamellae has been observed [25]. However, we hypothesized that the interactions between collagen fibers within a lamella would be stronger and more numerous due to the proximity of the fibers to one another. A third assumption was that the mechanical response of the crosslinks is limited to a resistance to shear stress in the direction of the fibers, while in reality the response of the crosslinks is certainly more complex. For example, the crosslinks are likely able to resist a tensile load transverse to the fiber direction. In a two fiber family material such as the annulus, however, such a load would be primarily carried by the fibers in the adjacent lamellae, not by the crosslinks. Finally, we assumed no residual stresses, although the constituents of

biological tissues generally exist in a state of stress even when no external load is applied. For example, in an unloaded test specimen of the annulus, the proteoglycans exert a swelling pressure on the collagen fibers and place them in a state of tension. Future studies may provide data that will allow for a more accurate analysis of the residual stress states.

Recently, Elliott and Setton proposed a linear strain energy function for the annulus and associated particular linear invariants with fiber–matrix or fiber–fiber interactions [8,9]. They demonstrated a large contribution to the total strain energy from a fiber–fiber interaction term that is a function of the linearized form of the invariant I_8 (see Eq. (4)). We considered a similar approach by formulating the interactions term in Eq. (5) as a function of I_8 rather than basing this term on the mechanical shear response of the crosslinks. This approach achieved good results in predicting the experimental data that were qualitatively similar to those that we have presented here. We ultimately chose to model the interactions term on the shear response of the crosslinks because we could not readily relate I_8 to a structural interaction of the tissue. The invariant I_8 is identically zero whenever $\phi = 45^\circ$, therefore basing the interactions term on I_8 leads to the implausible prediction that a composite material with orthogonally oriented fibers lacks fiber–fiber interactions that are available to all other two-fiber family composites. Additionally, this invariant exists for a material with two fiber families but an equivalent does not exist in a one fiber family material, therefore this quantity does not represent interactions between the densely packed collagen fibers within a single annular lamella.

We modeled the material behavior of the annulus fibrosus using an orthotropic continuum model with separate terms to represent the contributions of the annular constituents. One advantage to this approach is that we can associate particular physical characteristics to the parameters of the strain energy function. For example, ϕ represents the angle of the fiber orientation, and we can model another specimen (from the inner annulus, for example) which differs only by the fiber angle by changing just the value of ϕ [9]. Future studies may allow us to correlate the strain energy coefficients with biochemical measures. For example, we may be able to correlate proteoglycan content with the material parameters a_1 and a_2 , collagen content with a_3 , and collagen crosslink density with a_4 , allowing us to gain insight into the relationship between the biochemistry and the mechanical properties of the healthy and degenerated annulus.

In conclusion, our results highlight some important considerations for the biomechanical testing of soft tissues. In order to develop experimental datasets that have continuous elastic moduli at the tension/compression transition, the same reference configuration must be

identified and implemented in both test protocols. Our new experimental results allowed us to write a constitutive formulation for the annulus fibrosus that accurately depicts the mechanical response to multiple experimental deformations. We accomplished this with a strain energy function with additive terms meant to represent separate contributions from annular constituents. We anticipate that this formulation may be used in the future to more accurately predict the complex annular stress and strain states and to elucidate structure–function relationships in the annulus fibrosus.

Acknowledgement

This research was sponsored by funding from the National Institutes of Health (AR44179).

References

- [1] Bass EC. Biaxial nonlinear elastic response of the human lumbar annulus fibrosus and its role in the determination of a physiologically relevant constitutive relation, PhD dissertation. Mechanical Engineering, University of California at Berkeley, Berkeley, CA, 1999.
- [2] Bass EC, Ashford FA, Segal MR, Lotz JC. Biaxial testing of human annulus fibrosus and its implications for a constitutive formulation. *Ann Biomed Eng*, submitted for publication.
- [3] Broom ND, Silyn-Roberts H. Collagen–collagen versus collagen–proteoglycan interactions in the determination of cartilage strength. *Arthritis Rheumat* 1990;33:1512–7.
- [4] Cassidy JJ, Hiltner A, Baer E. Hierarchical structure of the intervertebral disc. *Connect Tissue Res* 1989;23:75–88.
- [5] Duncan NA, Lotz JC. Experimental validation of a porohyperelastic finite element model of the annulus fibrosus. In: Middleton J, Jones ML, Pande GN, editors. *Computer methods in biomechanics and biomedical engineering*. Gordon and Breach; 1998.
- [6] Ebara S, Iatridis JC, Setton LA, Foster RJ, Mow VC, Weidenbaum M. Tensile properties of nondegenerate human lumbar annulus fibrosus. *Spine* 1996;21:452–61.
- [7] Eberlein R, Holzapfel GA, Schulze-Bauer CAJ. An anisotropic constitutive model for annulus tissue and enhanced finite element analyses of intact lumbar disc bodies. *Comput Meth Biomech Biomed Eng* 2001;4:209–30.
- [8] Elliott DM, Setton LA. A linear material model for fiber-induced anisotropy of the annulus fibrosus. *J Biomech Eng* 2000;122:173–9.
- [9] Elliott DM, Setton LA. Anisotropic and inhomogeneous tensile behavior of the human annulus fibrosus: experimental measurement and material model predictions. *J Biomech Eng* 2001;123:256–63.
- [10] Fujita Y, Duncan NA, Lotz JC. Radial tensile properties of the lumbar annulus fibrosus are site and degeneration dependent. *J Orthop Res* 1997;15:814–9.
- [11] Fujita Y, Wagner DR, Biviji AA, Duncan NA, Lotz JC. Anisotropic shear behavior of the annulus fibrosus: effect of harvest site and tissue pre-strain. *Med Eng Phys* 2000;22:349–57.
- [12] Fung YCB. Elasticity of soft tissues in simple elongation. *Am J Physiol* 1967;213:1532–44.
- [13] Holzapfel GA, Gasser TC, Ogden RW. A new constitutive framework for arterial wall mechanics and a comparative study of material models. *J Elasticity* 2000;61:1–48.
- [14] Hukins DWL. Disc structure and function. In: Ghosh P, editor. *The biology of the intervertebral disc*. Boca Raton, FL: CRC Press, Inc; 1988.
- [15] Iatridis JC, Kumar S, Foster RJ, Weidenbaum M, Mow VC. Shear mechanical properties of human lumbar annulus fibrosus. *J Orthop Res* 1999;17:732–7.
- [16] Kenedi RM, Gibson T, Daly CH. Bio-engineering studies of the human skin. The effects of unidirectional tension. In: Jackson SF, Harkness RD, Partridge SM, Tristman GR, editors. *Structure and function of connective and skeletal tissue*. London: Butterworths; 1965.
- [17] Klisch SM, Lotz JC. Application of a fiber-reinforced continuum theory to multiple deformations of the annulus fibrosus. *J Biomech* 1999;32:1027–36.
- [18] Klisch SM, Lotz JC. A special theory of biphasic mixtures and experimental results for human annulus fibrosus tested in confined compression. *J Biomech Eng* 2000;122:180–8.
- [19] Marchand F, Ahmed AM. Investigation of the laminate structure of lumbar disc annulus fibrosus. *Spine* 1990;15:402–10.
- [20] Neptune RR. Optimization algorithm performance in determining optimal controls in human movement analyses. *J Biomech Eng* 1999;121:249–52.
- [21] Panjabi MM. The stabilizing system of the spine. Part II. Neutral zone and instability hypothesis. *J Spinal Disorders* 1992;5:390–7.
- [22] Quapp KM, Weiss JA. Material characterization of human medial collateral ligament. *J Biomech Eng* 1998;120:757–63.
- [23] Spencer AJM. *Continuum theory of the mechanics of fibre-reinforced composites*. New York: Springer-Verlag; 1984.
- [24] Thompson JP, Pearce RH, Schechter MT, Adams ME, Tsang IKY, Bishop PB. Preliminary evaluation of a scheme for grading the gross morphology of the human intervertebral disc. *Spine* 1990;15:411–5.
- [25] Tsuji H, Hirano N, Ohshima H, Ishihara H, Terahata N, Motoe T. Structural variation of the anterior and posterior annulus fibrosus in the development of human lumbar intervertebral disc. *Spine* 1993;18:204–21.
- [26] Wagner DR, Lotz JC. *A non-linear anisotropic strain energy function for the annulus fibrosus*. San Francisco: Orthopaedic Research Society; 2001.
- [27] Wagner DR, Lotz JC. Selection of the zero-stress state affects nonlinear material response. Dallas, TX: Orthopaedic Research Society; 2002.
- [28] Weiss JA, Maker BN, Govindjee S. Finite element implementation of incompressible, transversely isotropic hyperelasticity. *Comput Meth Appl Mech Eng* 1996;135:107–28.
- [29] Wu H, Yao R. Mechanical behavior of the human annulus fibrosus. *J Biomech* 1976;9:1–7.